Figure 1. Structural Observations

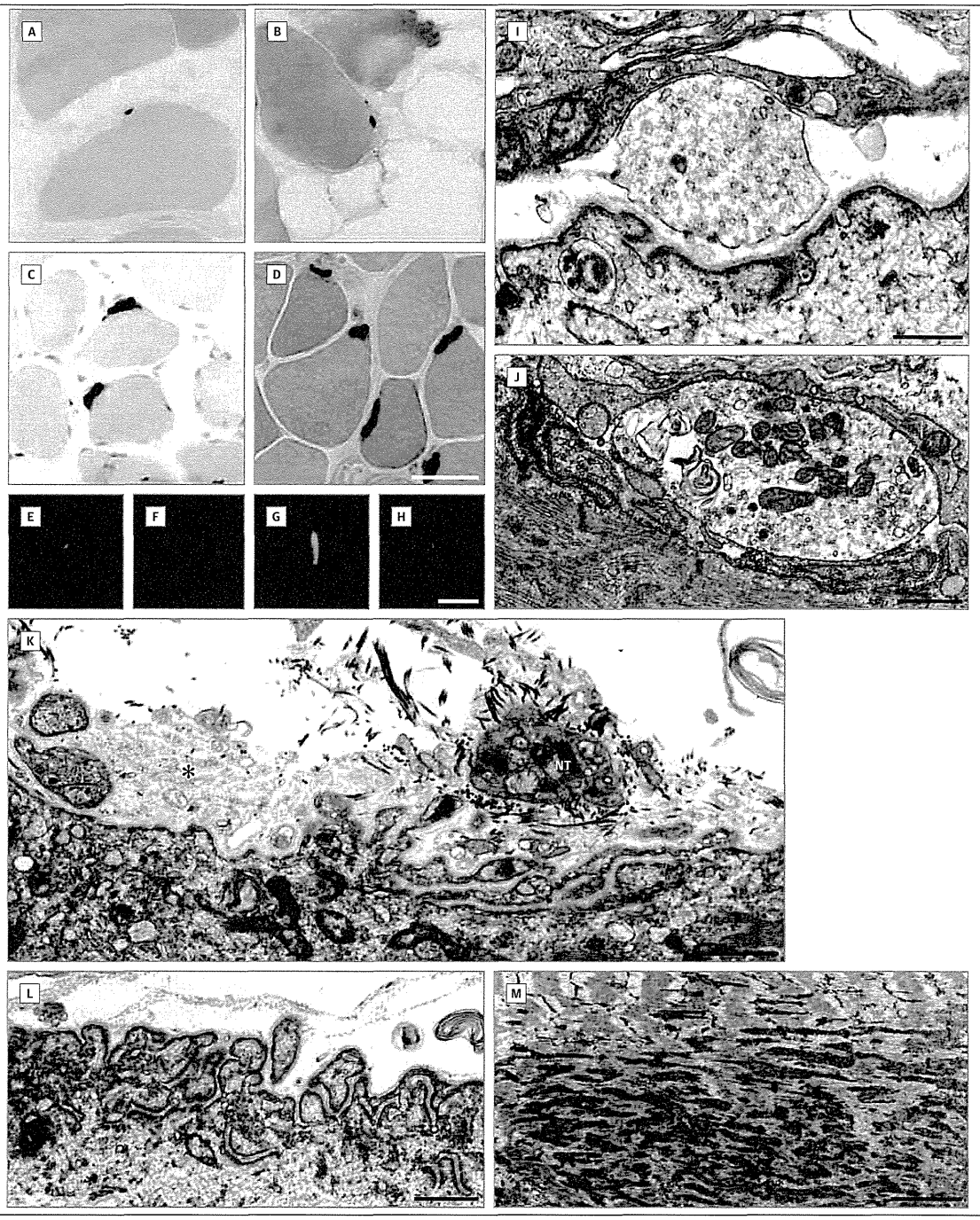

In transverse sections, the length of acetylcholinesterase (AChE)–reacted end-plate (EP) regions is markedly reduced in the EPs of patient 1 (A and B) compared with the EPs of control participants (C and D). Paired fluorescence studies reveal reduced expression of AChE (green) and acetylcholine receptors (AChRs) (red) in the EPs of patient 1 (E and F) compared with the EPs of control participants (G and H). Electron microscopy reveals simplified postsynaptic regions (I and J) and patchy expression of AChRs (black reaction product) at the EP (J). K, Electron microscopy also reveals a degenerating nerve terminal (NT) separated from a shallow postsynaptic region by a synaptic space containing coarse collagen fibrils; the region on the left shows a degenerate postsynaptic region displaying basal lamina remnants of preexisting folds (asterisk) and no NT. Electron microscopy also reveals a noninnervated postsynaptic region (L) and focal myofibrillar degeneration (M). Scale bars: A-D, 50 μm; E-H, 20 μm; I-L, 1 μm; M, 2 μm.

Table 1. Quantitative Analysis of Single EP Regions[a]

Measure	Control Participants (n = 15) Mean (SE)	EP Regions, No.	Older Sister Mean (SE)	EP Regions, No.	P Value
Nerve terminal area, μm^2	3.88 (0.39)	63	3.19 (0.76)	11	.59
Postsynaptic membrane length, μm	54.9 (5.3)	47	18.2 (2.00)	15	<.001
Postsynaptic area, μm^2	10.6 (0.79)	59	7.07 (1.02)	15	<.05
Postsynaptic membrane density, μm/μm^2	5.83 (0.25)	47	2.88 (0.23)	15	<.001

[a] More than 1 region can occur at a single end plate (EP).

Table 2. Microelectrode Studies of Neuromuscular Transmission and α-bgt Binding Sites per EP

Measure	Control Participants (n = 13) Mean (SE)	Participants or EPs,[a] No.	Older Sister Mean (SE)	EPs, No.	P Value[b]
EPP amplitude, mV	28.76 (1.98)	10[c]	4.66 (0.74)	13	<.001
MEPP amplitude, mV	1.00 (0.03)	165[d]	0.43 (0.078)	13[e]	<.001
Quantal content of EPP at 1 Hz (*m*)[f]	26.9 (1.0)	91	10.8 (2.36)	13	<.001
[^{125}I]α-bgt binding sites per EP, No.	12.8 × 10^6 (0.8 × 10^6)	13	3.03 × 10^6	1	<.001[g]

Abbreviations: EP, end plate; [^{125}I]α-bgt, iodine 125–labeled α-bungarotoxin; MEPP, miniature EP potential.

[a] Number of participants for EPP amplitudes and [^{125}I]α-bgt binding sites, and number of EPs for MEPP and *m*.

[b] Determined by use of 2-tailed *t* test.

[c] Control EPP amplitudes estimated from the product of *m* and the MEPP amplitude.

[d] Corrected for a membrane potential of −80 mV and a fiber diameter of 50 μm (30°C).

[e] Estimated from quantal component of EPP.

[f] Corrected for a membrane potential of −80 mV, nonlinear summation, and non-Poisson release.

[g] Determined by use of 1-sample 1-tailed *t* test.

terminal (Figure 1K and L) and 2 regions displaying degenerating junctional folds (Figure 1K). In contrast, at 157 EP regions of control participants, only 15 postsynaptic regions were unoccupied by the nerve terminal ($P < .001$, determined by use of the rank sum test), and only 6 postsynaptic regions displayed degenerating folds ($P < .03$, determined by use of the *z* score). Most postsynaptic regions had poorly developed junctional folds (Figure 1I and J), and a single nerve terminal was degenerating (Figure 1K). The postsynaptic reaction for AChR, revealed by peroxidase-labeled α-bungarotoxin, was attenuated (Figure 1J). At the light microscopic level, the intercostal muscle specimen showed a single-target formation and small focal decreases of enzyme activity. Consistent with this, at the electron microscopic level, occasional muscle fibers displayed focal myofibrillar degeneration (Figure 1M) that is likely secondary to functional denervation. Morphometric analysis revealed that the size of the nerve terminal was not significantly different from normal but that the postsynaptic area was reduced by 33% (ie, 67% of normal) and that the postsynaptic membrane density was reduced by 50% (ie, 50% of normal) (**Table 1**).

In Vitro Analysis of Neuromuscular Transmission

The evoked EPPs were subthreshold to trigger action potentials and were recorded without curare. The mean values for the EPP amplitude, the quantal content of the EPP (*m*), and the amplitude of the MEPP derived from the quantal component of the EPP were reduced to 16%, 40%, and 43%, respectively, of the corresponding mean values for the control participants. The mean number of AChRs per EP, determined from the number of α-bungarotoxin binding sites, was decreased to 25% of the mean number for the control participants (**Table 2**).

Mutation Analysis

Whole-exome sequencing in both patients (confirmed by Sanger sequencing) revealed a novel homozygous p.Glu1233Ala (c.3698A>C) mutation in exon 26 (**Figure 2**). The mutated residue is positioned at the edge of the third β-propeller domain of LRP4 and close to the conserved YWTD motif important for β-sheet formation. The unaffected brother and the mother are heterozygous for the mutation. Glu1233 is highly conserved across vertebrates, but not in insects, and is not reported in the Exome Variant Database (Exome Variant Server, National Heart, Lung, and Blood Institute Grand Opportunity Exome Sequencing Project, Seattle, Washington [http://evs.gs.washington.edu/EVS/]; January 2015), and it is predicted to be disease causing by MutationTaster but benign by Polymorphism Phenotyping v2. Interestingly, mutations in the central cavity of the third β-propeller domain of *LRP4* were previously reported to impair Wnt signaling and cause bone disease, including Cenani-Lenz syndactyly syndrome[25] and sclerosteosis-2.[26]

Because the A>C variant is the penultimate nucleotide of exon 26 and because MutationTaster predicts it to alter splicing, we isolated cDNA from the patient's intercostal and serratus anterior muscles and amplified the segment, including exon 26 by 2 different sets of primers. In both specimens, the mutant residue was homozygous, and there was no evidence for abnormal splicing.

Figure 2. Structure of and Identified Mutations in *LRP4*

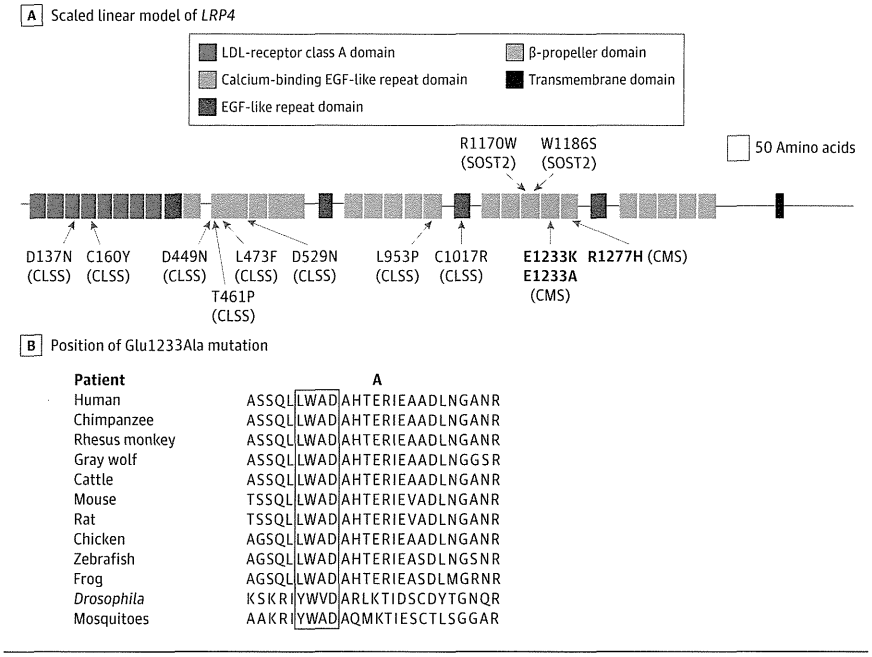

A, Scaled linear model of *LRP4* with color-coded domains and identified mutations. Mutations causing congenital myasthenic syndrome (CMS) are shown in red letters; mutations causing Cenani-Lenz syndactyly syndrome (CLSS) and sclerosteosis-2 (SOST2) are shown in black letters. B, The Glu1233Ala mutation is in a highly conserved domain of *LRP4* and the blue box encloses a motif conserved in all species. The substituting Ala, indicated by the red A, is 4 residues downstream of this motif. Glu1233 is highly conserved across vertebrates but not in insects. EGF indicates epidermal growth factor.

Expression Studies

Expression studies show that Glu1233Ala inhibits the MuSK signaling pathway. During the formation of the neuromuscular junction, binding of agrin to LRP4 induces phosphorylation and activation of MuSK.[3] Activated MuSK activates ATF2 downstream of JNK to induce clustering of AChRs.[12,27] To investigate the effect of the Glu1233Ala mutation on this signaling pathway, we used a JNK-responsive ATF2-luc reporter that specifically monitors MuSK-dependent stimulation in transfected HEK293 cells.[27] When LRP4 and MuSK are overexpressed, limited ATF2 activation occurs even in the absence of agrin.[12] The addition of agrin to this system further enhances ATF2 activation by wild-type LRP4, whereas activation of ATF2 by mutant LRP4 is markedly attenuated (**Figure 3**A). We found that both the previously reported Glu1233Lys mutation[12] (Figure 3B) and the currently identified Glu1233Ala mutation (Figure 3A) compromise ATF2 activation, but the activation is consistently lower with Glu1233Ala than with Glu1233Lys.

In another experiment using HEK293 cells, we examined the effects of wild-type and mutant LRP4 on MuSK phosphorylation that occurs during the assembly of the agrin-LRP4-MuSK complex. Consistent with its effects on MuSK signaling activity, mutant LRP4 compromises agrin-enhanced MuSK phosphorylation (Figure 3C). Both experiments support the notion that Glu1233Ala in LRP4 compromises agrin-mediated activation of MuSK.

MuSK and agrin bind to different extracellular residues of LRP4.[3] We therefore examined the binding of MuSK and agrin to mutant and wild-type LRP4 expressed on the surface of COS cells. We first confirmed that both wild-type and mutant LRP4 are similarly expressed on the plasma membrane by use of the biotinylation assay (Figure 3D). We then overlaid recombinant human MuSKect-AP and recombinant human neural agrin-AP on COS cells expressing LRP4. Measurement of alkaline phosphatase activity revealed that MuSK and agrin bind efficiently to wild-type LRP4 but not to mutant LRP4 (Figure 3E). Thus, all 3 experiments indicate that Glu1233Ala in LRP4 inhibits agrin-mediated upregulation of MuSK signaling.

Discussion

The 2 sisters described in this report harbor a homozygous p.Glu1233Ala mutation in the third propeller domain of LRP4 that binds to and activates MuSK. An intercostal muscle biopsy of the older sister revealed very small EPs with poorly developed postsynaptic regions, and postsynaptic regions that were degenerating or denuded of their nerve terminal. The amplitude of the EPP was reduced to 16% of normal owing to the combined decrease of the quantal content of the EPP and of the MEPP amplitude (Table 2). The decreased amplitude of the MEPP can be attributed to decreased input resistance of the EP owing to simplification of the postsynaptic membrane, as well as the attenuated expression of AChRs on the remaining junctional folds. The decreased quantal content of the EPP is adequately explained by the small size of individual EPs, and hence of the total number of synaptic vesicles available for release by nerve impulse. Thus, the observed structural and electrophysiologic abnormalities are consistent with an abrogated role played by LRP4 in the development and maintenance of the neuromuscular junction.[3]

Figure 3. Expression Studies

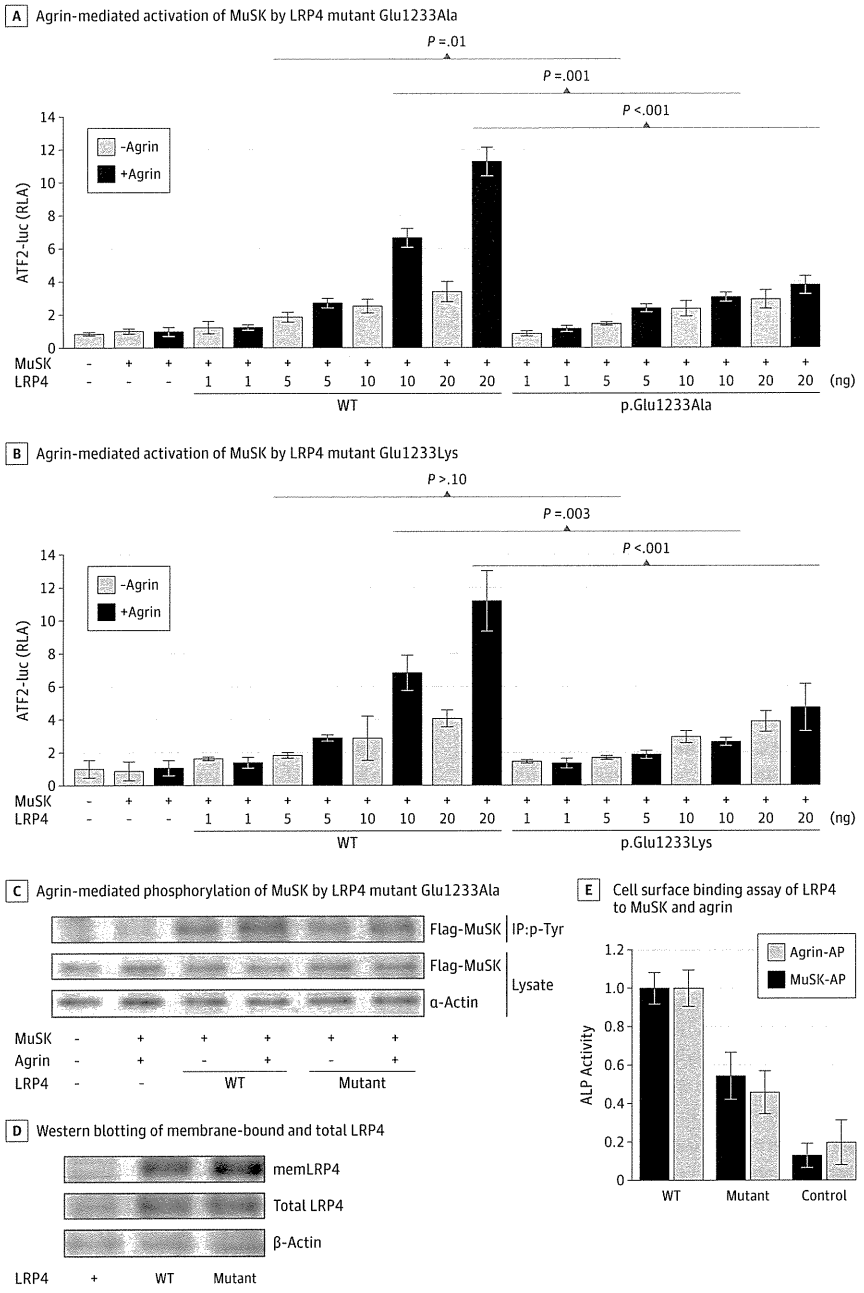

The lipoprotein receptor-related protein 4 (LRP4) mutants Glu1233Ala (A) and Glu1233Lys (B) inhibit agrin-mediated upregulation of muscle-specific tyrosine kinase (MuSK) signaling. Agrin-mediated upregulation of MuSK signaling in HEK293 cells is monitored by the ATF2-luciferase (ATF2-luc) reporter assay. Cells were transfected with the ATF2-luc and Renilla reporter plasmids, along with MuSK complementary DNA (cDNA) and wild-type (WT) or mutant LRP4, and then incubated with or without 10 ng/mL of agrin. Error bars indicate mean (SD) values (n=3) of relative luciferase activity (RLA) calculated by dividing the firefly luciferase activity by the Renilla luciferase activity, which is further normalized for activity without MuSK and LRP4. C, Effect of mutant and WT LRP4 on MuSK phosphorylation in HEK293 cells transfected with Flag-MuSK and the indicated LRP4 cDNA with or without agrin (10 ng/mL). Phosphorylated MuSK was detected by immunoprecipitation of cell lysate by antiphosphotyrosine antibody (IP:p-Tyr) followed by immunoblotting with anti-FLAG antibody. Wild-type LRP4 phosphorylates MuSK, which is further enhanced by agrin. Mutant LRP4 abolished responsiveness to agrin. D, Western blotting detected membrane-bound LRP4 (memLRP4) and total LRP4. Membrane proteins were biotinylated and precipitated with streptavidin. β-Actin in each sample serves as a loading control. E, The LRP4 mutant impairs binding of LRP4 to MuSK and agrin in cell surface binding assays. COS7 cells were transfected with the WT or mutant LRP4 cDNA and treated with a concentrated conditioned medium containing either neural agrin-mycAP or MuSKect-mycAP, both of which expressed an alkaline phosphatase (ALP) fusion protein. Control cells were transfected with an empty vector. The error bars indicate mean (SD) of ALP activity of bound agrin-mycAP and MuSKect-mycAP in 3 independent wells. Mutant LRP4 reduces binding of MuSKect-mycAP and agrin-mycAP.

Conclusions

The first reported patient with LRP4-related myasthenia harbored 2 heterozygous mutations in LRP4, p.Glu1233Lys and p.Arg1277His. At 14 years of age, her synaptic contacts were dysplastic, the individual EP regions were smaller than normal, and the EP AChR content slightly reduced, but, paradoxically, in vitro electrophysiology studies of intercostal muscle EPs revealed no abnormality.[12] Interestingly, expression studies of both mutant proteins in the first patient[12] and of the single mutant protein in the 2 sisters in this study revealed impaired LRP4 binding to, activating, and phosphorylating MuSK. The reason for the much milder clinical, structural, and electrophysiologic abnormalities observed in the first identified patient with LRP4-related myasthenia compared with the patients described in this report remains unknown. We initially attributed the milder findings in the first reported patient to

relative sparing of the intercostal muscles. Alternatively, the structural and physiologic abnormalities at the EPs in LRP4-related myasthenia could worsen with age, consistent with the progressive clinical course in all 3 LRP4-deficient patients observed to date. The greater suppression of ATF2 activation by the Glu1233Ala mutation in LRP4 than by the previously reported Glu1233Lys mutation in LRP4 likely also contributes to the phenotypic differences between the first reported patient and the 2 patients described herein. Finally, single-nucleotide polymorphisms in modifier genes may also contribute to phenotypic differences. That both kinships harbor mutations at the edge of the third β-propeller domain and that 2 of the 3 identified mutations occur at codon 1233 suggest a hot spot for causing CMS.

ARTICLE INFORMATION

Accepted for Publication: April 6, 2015.

Published Online: June 8, 2015. doi:10.1001/jamaneurol.2015.0853.

Author Contributions: Dr Engel had full access to all of the data in the study and takes responsibility for the integrity of the data and the accuracy of the data analysis.
Study concept and design: Selcen, Shen, Ohno, Engel.
Acquisition, analysis, or interpretation of data: All authors.
Drafting of the manuscript: Selcen, Ohno, Engel.
Critical revision of the manuscript for important intellectual content: All authors.
Statistical analysis: Shen, Engel.
Obtained funding: Selcen, Ohkawara, Ohno, Engel.
Administrative, technical, or material support: Ohno, Engel.
Study supervision: Ohno, Engel.

Conflict of Interest Disclosures: None reported.

Funding/Support: This work was supported by National Institutes of Health grant NS62777 (Dr Engel), the Mayo Clinic Center for Individualized Medicine, and by Grants-in-Aid from the Ministry of Education, Culture, Sports, Science and Technology and Ministry of Health, Labour and Welfare of Japan (Drs Ohkawara and Ohno).

Role of Funder/Sponsor: The funding sources had no role in the design and conduct of the study; collection, management, analysis, or interpretation of the data; preparation, review, or approval of the manuscript; and decision to submit the manuscript for publication.

REFERENCES

1. Kim N, Stiegler AL, Cameron TO, et al. Lrp4 is a receptor for Agrin and forms a complex with MuSK. *Cell*. 2008;135(2):334-342.

2. Zhang B, Luo S, Wang Q, Suzuki T, Xiong WC, Mei L. LRP4 serves as a coreceptor of agrin. *Neuron*. 2008;60(2):285-297.

3. Burden SJ, Yumoto N, Zhang W. The role of MuSK in synapse formation and neuromuscular disease. *Cold Spring Harb Perspect Biol*. 2013;5(5):a009167.

4. Huzé C, Bauché S, Richard P, et al. Identification of an agrin mutation that causes congenital myasthenia and affects synapse function. *Am J Hum Genet*. 2009;85(2):155-167.

5. Maselli RA, Fernandez JM, Arredondo J, et al. LG2 agrin mutation causing severe congenital myasthenic syndrome mimics functional characteristics of non-neural (z-) agrin. *Hum Genet*. 2012;131(7):1123-1135.

6. Nicole S, Chaouch A, Torbergsen T, et al. Agrin mutations lead to a congenital myasthenic syndrome with distal muscle weakness and atrophy. *Brain*. 2014;137(pt 9):2429-2443.

7. Chevessier F, Faraut B, Ravel-Chapuis A, et al. MUSK, a new target for mutations causing congenital myasthenic syndrome. *Hum Mol Genet*. 2004;13(24):3229-3240.

8. Mihaylova V, Salih MA, Mukhtar MM, et al. Refinement of the clinical phenotype in musk-related congenital myasthenic syndromes. *Neurology*. 2009;73(22):1926-1928.

9. Maselli RA, Arredondo J, Cagney O, et al. Mutations in MUSK causing congenital myasthenic syndrome impair MuSK-Dok-7 interaction. *Hum Mol Genet*. 2010;19(12):2370-2379.

10. Ben Ammar A, Soltanzadeh P, Bauché S, et al. A mutation causes MuSK reduced sensitivity to agrin and congenital myasthenia. *PLoS One*. 2013;8(1):e53826.

11. Maggi L, Brugnoni R, Confalonieri P, et al. Marked phenotypic variability in two siblings affected by congenital myasthenic syndrome caused by mutations in MUSK. *J Neurol*. 2013;260(11):2894-2896.

12. Ohkawara B, Cabrera-Serrano M, Nakata T, et al. LRP4 third β-propeller domain mutations cause novel congenital myasthenia by compromising agrin-mediated MuSK signaling in a position-specific manner. *Hum Mol Genet*. 2014;23(7):1856-1868.

13. Fambrough DM, Engel AG, Rosenberry TL. Acetylcholinesterase of human erythrocytes and neuromuscular junctions: homologies revealed by monoclonal antibodies. *Proc Natl Acad Sci U S A*. 1982;79(4):1078-1082.

14. Engel AG. The muscle biopsy. In: Engel AG, Franzini-Armstrong C, eds. *Myology*. 3rd ed. New York, NY: McGraw-Hill; 2004:681-690.

15. Engel AG. Quantitative morphological studies of muscle. In: Engel AG, Franzini-Armstrong C, eds. *Myology*. 2nd ed. New York, NY: McGraw-Hill; 1994:1018-1045.

16. Engel AG, Lindstrom JM, Lambert EH, Lennon VA. Ultrastructural localization of the acetylcholine receptor in myasthenia gravis and in its experimental autoimmune model. *Neurology*. 1977;27(4):307-315.

17. Engel AG. The investigation of congenital myasthenic syndromes. *Ann N Y Acad Sci*. 1993;681:425-434.

18. Elmqvist D, Quastel DMJ. A quantitative study of end-plate potentials in isolated human muscle. *J Physiol*. 1965;178(3):505-529.

19. Engel AG, Nagel A, Walls TJ, Harper CM, Waisburg HA. Congenital myasthenic syndromes: I, deficiency and short open-time of the acetylcholine receptor. *Muscle Nerve*. 1993;16(12):1284-1292.

20. Uchitel O, Engel AG, Walls TJ, Nagel A, Atassi MZ, Bril V. Congenital myasthenic syndromes: II, syndrome attributed to abnormal interaction of acetylcholine with its receptor. *Muscle Nerve*. 1993;16(12):1293-1301.

21. Weston C, Yee B, Hod E, Prives J. Agrin-induced acetylcholine receptor clustering is mediated by the small guanosine triphosphatases Rac and Cdc42. *J Cell Biol*. 2000;150(1):205-212.

22. Gupta S, Campbell D, Dérijard B, Davis RJ. Transcription factor ATF2 regulation by the JNK signal transduction pathway. *Science*. 1995;267(5196):389-393.

23. Harper CM. Electrodiagnosis of myasthenic disorders. In: Engel AG, et al. *Myasthenia Gravis and Myasthenic Disorders*. 2nd ed. New York, NY: Oxford; 2012:37-59.

24. Herrmann DN, Horvath R, Sowden JE, et al. Synaptotagmin 2 mutations cause an autosomal-dominant form of Lambert-Eaton myasthenic syndrome and nonprogressive motor neuropathy [published correction appears in *Am J Hum Genet*. 2014;95(4):472]. *Am J Hum Genet*. 2014;95(3):332-339.

25. Li Y, Pawlik B, Elcioglu N, et al. LRP4 mutations alter Wnt/beta-catenin signaling and cause limb and kidney malformations in Cenani-Lenz syndrome. *Am J Hum Genet*. 2010;86(5):696-706.

26. Leupin O, Piters E, Halleux C, et al. Bone overgrowth-associated mutations in the *LRP4* gene impair sclerostin facilitator function. *J Biol Chem*. 2011;286(22):19489-19500.

27. Ohkawara B, Niehrs C. An ATF2-based luciferase reporter to monitor non-canonical Wnt signaling in *Xenopus* embryos. *Dev Dyn*. 2011;240(1):188-194.

SCIENTIFIC REPORTS

OPEN

SRSF1 and hnRNP H antagonistically regulate splicing of *COLQ* exon 16 in a congenital myasthenic syndrome

Received: 24 March 2015
Accepted: 22 July 2015
Published: 18 August 2015

Mohammad Alinoor Rahman[1], Yoshiteru Azuma[1], Farhana Nasrin[1], Jun-ichi Takeda[1], Mohammad Nazim[1], Khalid Bin Ahsan[1], Akio Masuda[1], Andrew G. Engel[2] & Kinji Ohno[1]

The catalytic subunits of acetylcholinesterase (AChE) are anchored in the basal lamina of the neuromuscular junction using a collagen-like tail subunit (ColQ) encoded by *COLQ*. Mutations in *COLQ* cause endplate AChE deficiency. An A-to-G mutation predicting p.E415G in *COLQ* exon 16 identified in a patient with endplate AChE deficiency causes exclusive skipping of exon 16. RNA affinity purification, mass spectrometry, and siRNA-mediated gene knocking down disclosed that the mutation disrupts binding of a splicing-enhancing RNA-binding protein, SRSF1, and *de novo* gains binding of a splicing-suppressing RNA-binding protein, hnRNP H. MS2-mediated artificial tethering of each factor demonstrated that SRSF1 and hnRNP H antagonistically modulate splicing by binding exclusively to the target in exon 16. Further analyses with artificial mutants revealed that SRSF1 is able to bind to degenerative binding motifs, whereas hnRNP H strictly requires an uninterrupted stretch of poly(G). The mutation compromised splicing of the downstream intron. Isolation of early spliceosome complex revealed that the mutation impairs binding of U1-70K (snRNP70) to the downstream 5′ splice site. Global splicing analysis with RNA-seq revealed that exons carrying the hnRNP H-binding GGGGG motif are predisposed to be skipped compared to those carrying the SRSF1-binding GGAGG motif in both human and mouse brains.

RNA splicing is a highly specialized process especially evolved in humans and other higher metazoans to achieve intricate regulation of gene expressions and to expand the proteome diversity. It is well established that misregulated splicing compromises the fidelity of biological processes and causes a plethora of human diseases. However, the precise molecular mechanisms of how a disease-causing mutation compromises the finely tuned splicing regulation have been dissected in only a limited number of genes. Elucidation of the mechanisms that cause abnormal splicing in human diseases also sheds light on the splicing code in the normal state, and can possibly lead to development of rational therapy.

Congenital myasthenic syndromes (CMSs) are a heterogeneous group of inherited neuromuscular disorders, which arise due to defects in genes encoding presynaptic, synaptic, and postsynaptic proteins expressed at the neuromuscular junction (NMJ)[1,2]. Acetylcholinesterase (AChE) encoded by *ACHE* rapidly terminates neuromuscular signal transmission by hydrolyzing the neurotransmitter acetylcholine (ACh). The predominant species of AChE at NMJ is the asymmetric A_{12} species[3] which comprises three tetramers of the $AChE_T$ isoform that are covalently attached to the triple helical collagen-like tail (ColQ). ColQ encoded by *COLQ* is essential for anchoring AChE to the NMJ. ColQ has three distinct domains: an N-terminal proline-rich domain organizing the catalytic AChE subunits into a tetramer, a collagen domain forming a triple helix and harboring two heparan-sulfate-proteoglycan-binding

[1]Division of Neurogenetics, Center for Neurological Diseases and Cancer, Nagoya University Graduate School of Medicine, Nagoya, Aichi, Japan. [2]Department of Neurology, Mayo Clinic, Rochester, MN, USA. Correspondence and requests for materials should be addressed to K.O. (email: ohnok@med.nagoya-u.ac.jp)

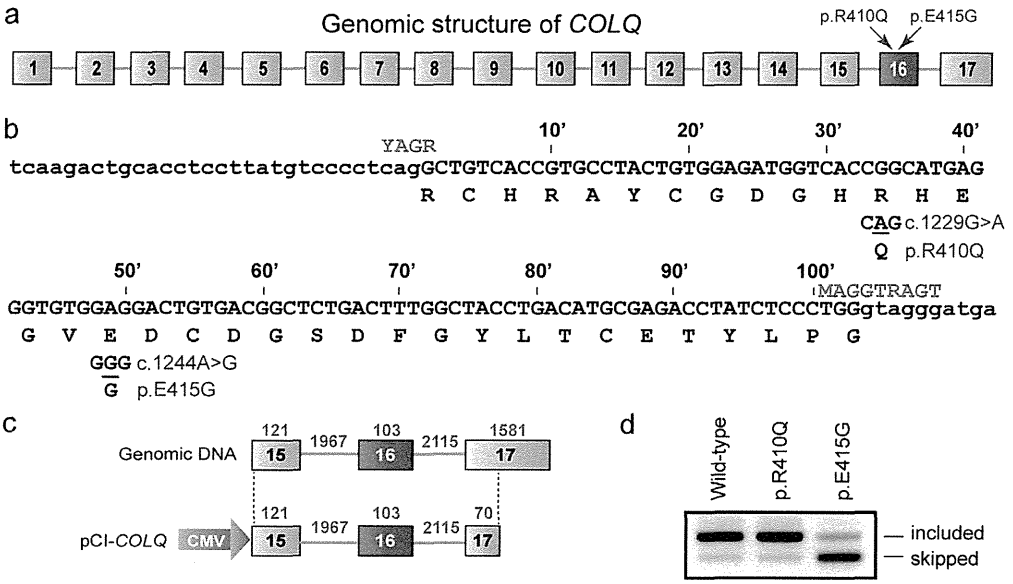

Figure 1. Genomic structure of *COLQ*, identified mutations, and their functional consequences. (**a**) Genomic structure (not drawn to scale) of human *COLQ* gene and two identified mutations in exon 16. (**b**) Nucleotide sequence of *COLQ* exon 16 (uppercase letters) and its flanking introns (lowercase letters). The two mutant nucleotides are underlined. Exonic positions are indicated above the sequence. The consensus sequences of U2-dependent 5′ splice site and 3′ splice site are shown in green letters (Y = C/T, R = A/G, M = A/C)[51]. (**c**) Structure of pCI-*COLQ* minigene. Genomic structure is not drawn to scale. The lengths of exons and introns are indicated in blue. (**d**) RT-PCR of *COLQ* minigene expressed in HeLa cells.

domains (HSPBD), and a C-terminal domain (CTD) enriched in charged amino acids and cysteines. Endplate AChE deficiency is caused by recessive mutations in the *COLQ* gene, but not by mutations in the *ACHE* gene encoding the catalytic subunit[4]. A number of mutations in *COLQ* are associated with endplate AChE deficiency[5]. Based on the position of the mutation and the effect on AChE expression, *COLQ* mutations can fall into four categories[6]: (1) N-terminal mutations compromising the association of $AChE_T$ with ColQ; (2) truncation mutations in the collagen domain disrupting the collagenic tail of AChE; (3) CTD missense mutations disrupting triple helical conformation of ColQ; and (4) CTD mutations affecting anchoring of ColQ at NMJ. We exploited specific binding of the HSPBD to perlecan[7] and of the CTD to MuSK[8] to develop a protein-anchoring therapy for *Colq*-knockout mice[9], but there is no rational therapy for human endplate AChE deficiency except for partial mitigation of the symptoms with ephedrine[10] or albuterol[11].

Serine/arginine-rich splicing factor 1 (SRSF1) is a ubiquitously expressed splicing factor of the serine (S)- and arginine (R)-rich protein family, which functions in both constitutive and alternative splicing[12]. SRSF1 also has a role in nonsense-mediated mRNA decay (NMD)[13], mRNA export[14], and translation[15]. *SRSF1* is also reported to be a proto-oncogene[16]. HnRNP H is a member of heterogeneous nuclear ribonucleoprotein (hnRNP) family, which has been reported to function exclusively in pre-mRNA splicing[17–20].

We previously reported a missense mutation (p.E415G) in the CTD of *COLQ* in a patient with endplate AChE deficiency, which causes aberrant skipping of a constitutively spliced exon 16 encoding a part of the ColQ CTD[21]. In this manuscript, we investigate the mechanism underlying aberrant exon skipping. We demonstrate that the mutation disrupts binding of a splicing-enhancing factor SRSF1, and gains a *de novo* binding affinity for a splicing-suppressing factor hnRNP H. We also find that the mutation impairs recruitment of U1 snRNP (U1-70K) to the downstream 5′ splice site.

Results

p.E415G in the CTD of ColQ causes skipping of exon 16. We previously reported two heteroallelic missense mutations in *COLQ* exon 16 in a patient with endplate AChE deficiency (Fig. 1a,b)[21]. We introduced p.R410Q (c.1229G > A) and p.E415G (c.1244A > G) into human *COLQ* cDNA and expressed mutant ColQ proteins in COS cells. We overlaid the purified mutant ColQ on the frog muscle sections, and found that p.R410Q caused loss of binding of ColQ to the frog endplate, whereas p.E415G had no effect on binding of ColQ to the frog endplate[21]. RT-PCR analysis revealed that p.E415G caused skipping of *COLQ* exon 16 in the patient muscle, indicating that p.E415G is not a missense mutation but a splicing mutation. Skipping of exon 16 (103 nt) causes a shift in the reading frame and deletes the C-terminal one-third of the CTD. We reported that similarly deleted or mutated CTDs are incompetent to bind to

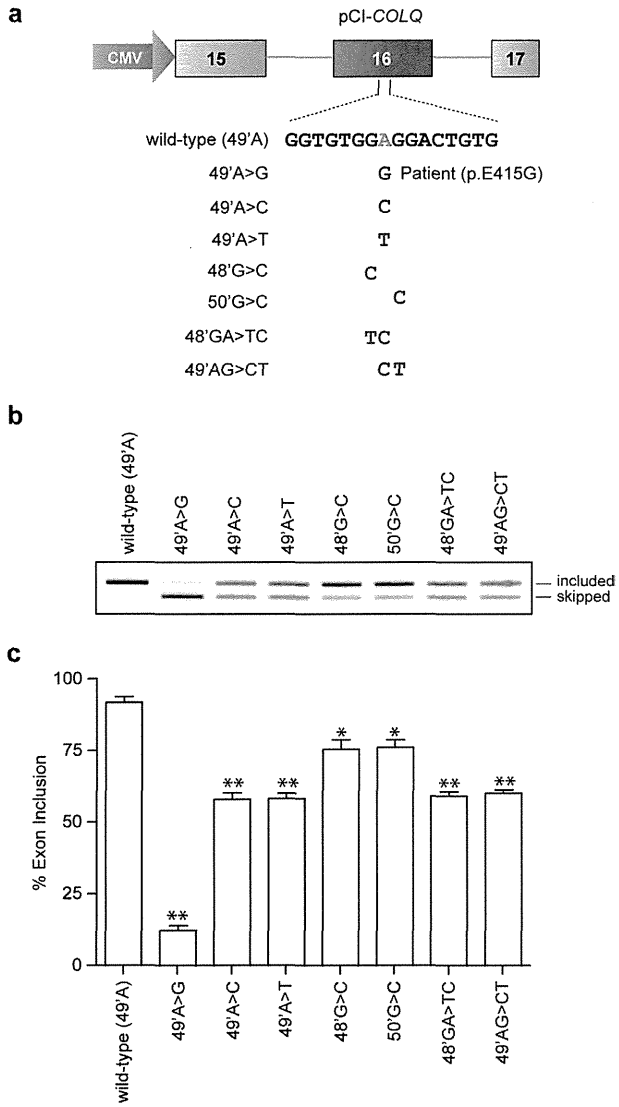

Figure 2. Construction of mutant minigenes and splicing assays. (**a**) Structure of pCI-*COLQ* minigene. The patient's mutation and six artificial mutations introduced into *COLQ* minigene are indicated. Exonic positions indicated in Fig. 1b are used. (**b**) RT-PCR of *COLQ* minigenes in HeLa cells. (**c**) Ratios of exon 16 inclusion are quantified with image J. Mean and standard deviation (SD) of three independent experiments are indicated. $^{**}p < 0.01$ and $^{*}p < 0.05$ compared to the wild-type minigene by Student's t-test.

MuSK and are incapable of being anchored to the NMJ[21,22]. In this study, we investigate the molecular basis of aberrant splicing due to p.E415G.

p.E415G disrupts an exonic splicing enhancer (ESE), and *de novo* generates an exonic splicing silencer (ESS). We first confirmed that a minigene spanning exons 15 and 17 expressed in HeLa cells recapitulates aberrant splicing (Fig. 1c,d). To examine whether the identified splicing mutation (p.E415G) disrupts an ESE or *de novo* generates an ESS, we engineered six artificial mutations at or around p.E415G (Fig. 2a). All mutants caused skipping of exon 16 with variable degrees (Fig. 2b,c), indicating that the A nucleotide at exonic position 49 and its neighboring nucleotides constitute an ESE. Among the analyzed mutations, the patient's mutation (G at exonic position 49) caused marked skipping of exon 16 compared to those observed with the other mutants, indicating that the patient's mutation possibly generates a *de novo* ESS.

p.E415G disrupts binding of SRSF1 and gains binding of hnRNP H. Having identified the essential nucleotides that constitute a splicing *cis*-element, we next searched for a splicing *trans*-factor responsible for splicing of exon 16. We employed RNA affinity purification of the HeLa nuclear extract with

an RNA probe carrying wild-type or mutant (p.E415G) sequence. Coomassie blue staining of the RNA affinity-purified proteins showed a ~30 kDa protein in the wild-type RNA probe but not in the p.E415G probe (Fig. 3b, open arrowhead). In addition, we noticed *de novo* binding of a ~55 kDa protein in the p.E415G probe (Fig. 3b, closed arrowhead). Mass spectrometry analysis of the excised bands disclosed that the molecule bound to the wild-type RNA probe was SRSF1, and that to the p.E415G RNA probe was hnRNP H. We confirmed the identity of bound proteins by immunoblotting with specific antibodies against SRSF1 (32–4500, Invitrogen) and hnRNP H (A300–511A, Bethyl Laboratories) (Fig. 3c). The immunoblotting indeed demonstrated that SRSF1 binds only to the wild-type probe, whereas hnRNP H binds only to the p.E415G probe.

SRSF1 enhances and hnRNP H silences inclusion of exon 16. We next examined the effects of SRSF1 and hnRNP H on splicing of exon 16 by siRNA-mediated downregulation of SRSF1 and hnRNP H in HeLa cells. SRSF1 and hnRNP H were efficiently downregulated in HeLa cells (Fig. 3d). Downregulation of SRSF1 induced exclusion of exon 16 in the wild-type minigene (Fig. 3e, lane 3), whereas downregulation of hnRNP H induced inclusion of exon 16 in the p.E415G minigene (Fig. 3e, lane 6), indicating that SRSF1 functions as a splicing enhancer for the wild-type minigene and hnRNP H functions as a splicing silencer for the p.E415G minigene. We observed similar splicing alterations with a second set of siRNAs targeting different sites of each mRNA in HeLa cells (Fig. S1a and b).

We next confirmed that SRSF1 and hnRNP H indeed work on the identified *cis*-element and not on the other sites. To this end, we tethered SRSF1 or hnRNP H to the target using the bacteriophage MS2 coat protein. We made an effector construct expressing MS2-tagged SRSF1 and hnRNP H proteins (MS2-SRSF1 and MS2-H, respectively), and the target minigene construct (pCI-*COLQ*-MS2), in which the MS2-binding site was substituted for the native target site. As expected, tethering of SRSF1 to the target induced inclusion of exon 16 (Fig. 3f, lane 4), whereas tethering of hnRNP H caused skipping of exon 16 (Fig. 3f, lane 6). Lack of the splicing modulating effects of SRSF1 and hnRNP H without the MS2-tag indicates that neither SRSF1 nor hnRNP H works at the other sites (Fig. 3f, lanes 3 and 5). We also confirmed that MS2 alone or MS2-fused hnRNP L (hnRNP L-MS2) had no effect on splicing of pCI-*COLQ*-MS2 (Fig. 3f, lanes 2 and 7). Thus, SRSF1 and hnRNP H exert splicing-enhancing and splicing-silencing activities exclusively on the identified target, respectively.

Molecular basis of binding of SRSF1 versus hnRNP H and splicing regulation. Previous reports suggest that SRSF1 binds to GA-rich sequence[12,23,24] and hnRNP H binds to poly(G) sequence[25–27]. The wild-type *COLQ* exon 16 harbors a motif of GGAGGA, and the patient's mutation (p.E415G) convert the GGAGG motif to GGGGG. We identified that SRSF1 binds to wild-type RNA probe, whereas hnRNP H binds to the p.E415G RNA probe. The GGAGG motif indeed matches to the functional SELEX consensus of SRSF1 [(G/C)(A/G)(G/C)A(G/C)GA][28], as well as to *in vivo* binding motifs 2 and 3 identified by CLIP-seq (cross-linked immunoprecipitation and deep sequencing)[12]. On the other hand, GGGGG motif also matches to the previously identified *in vitro* and *in vivo* binding motif of hnRNP H[25–27]. Therefore, a single nucleotide substitution switches binding of the splicing-enhancing SRSF1 to the splicing-suppressing hnRNP H, and causes aberrant splicing in patient's muscle.

We further dissected the molecular basis of splicing regulation by SRSF1 and hnRNP H. Analysis of artificial mutations showed that any mutations affecting the core GGAGG motif affected inclusion of exon 16 (Fig. 2). We therefore examined binding of SRSF1 and hnRNP H to the mutant RNA probes. RNA affinity purification followed by immunoblotting revealed that SRSF1 showed a strong binding affinity for GGAGG, and weak binding affinities for GGTGG and GGCGG (Fig. 4a,b). However, we did not detect binding of SRSF1 to GGGGG. In contrast, hnRNP H showed a strong binding affinity for GGGGG, whereas it could not bind to other motifs. The results of the binding assay were consistent with the splicing analysis of minigenes harboring these motifs (Fig. 2). To further confirm that SRSF1 and hnRNP H indeed regulate splicing of each motif, we overexpressed SRSF1 or hnRNP H in HeLa cells along with a minigene harboring each motif. As expected, SRSF1 exerted an additive effect on exon inclusion for minigenes harboring GGAGG (Fig. 4c), GGCGG (Fig. 4e) and GGTGG (Fig. 4f), to which SRSF1 was able to bind (Fig. 4b). On the contrary, SRSF1 had no effect on a minigene harboring GGGGG (Fig. 4d), to which SRSF1 could not bind. Similarly, overexpression of hnRNP H had no effect on GGAGG (Fig. 4c), GGCGG (Fig. 4e) and GGTGG (Fig. 4f), to which hnRNP H could not bind. In contrast, hnRNP H caused complete skipping of exon 16 harboring GGGGG (Fig. 4d), to which hnRNP H was able to bind (Fig. 4b). Therefore, binding of SRSF1 and hnRNP H to each motif (Fig. 4b) exerted the expected effects on splicing of exon 16 (Fig. 4c–f).

We next asked if there is any binding competition between hnRNP H and SRSF1 for the GGAGG or GGGGG motif, because the G nucleotide in the middle of the motif is an acceptable binding site for SRSF1[12]. For this purpose, we examined splicing of exon 16 of the wild-type (GGAGG) and p.E415G (GGGGG) minigenes after knocking down SRSF1 and/or hnRNP H. For the wild-type minigene, knockdown of SRSF1 alone and knockdown of both SRSF1 and hnRNP H showed similar degrees of exon skipping (Fig. 4g), indicating that hnRNP H had no effect on splicing of exon 16 even in the absence of SRSF1. Similarly, for the p.E415G minigene, SRSF1 had no effect on splicing of exon 16 even in the absence of hnRNP H (Fig. 4h). Taken together, lack of binding of SRSF1 to GGGGG and lack of binding of hnRNP H to GGAGG were not due to competition between SRSF1 and hnRNP H.

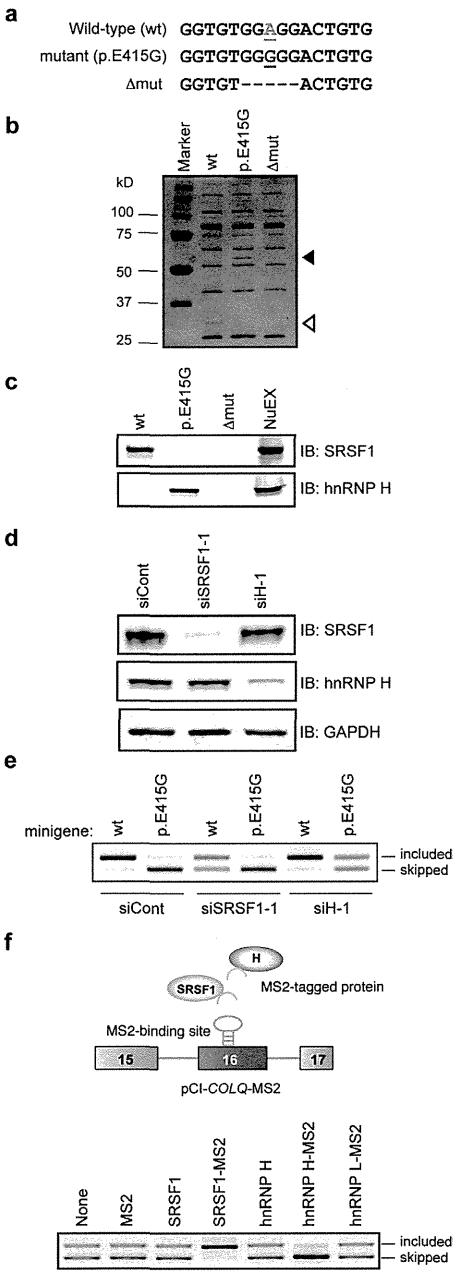

Figure 3. p.E415G compromises binding of a splicing-enhancing SRSF1 and gains binding of a splicing-suppressing hnRNP H. (**a**) Biotinylated RNA probes. (**b**) Coomassie blue staining of RNA affinity-purified products of HeLa nuclear extract. A ~30-kDa protein (open arrowhead) is detected only with the wild-type (wt) probe but not with the p.E415G or deletion mutant (Δmut) probe. In contrast, a ~55-kDa protein (closed arrowhead) is detected only with the p.E415G mutant. (**c**) Immunoblots (IB) of RNA affinity-purified proteins probed with indicated splicing *trans*-factors. The wild-type exon 16 (wt) binds to SRSF1and the p.E415G mutation disrupts its binding. The mutation gains *de novo* binding to hnRNP H. NuEX indicates 5% of the nuclear extract used in the assay. (**d**) Immunoblotting (IB) of HeLa cells treated with siRNA against control (siCont), SRSF1 (siSRSF1-1), and hnRNP H (siH-1) showing efficiency of siSRSF1-1 and siH-1. (**e**) RT-PCR of wild-type (wt) and p.E415G *COLQ* minigenes in HeLa cells treated with indicated siRNAs. A representative gel image of three independent experiments is shown. (**f**) Schematic presentation of a reporter minigene (pCI-*COLQ*-MS2) and *trans*-acting effectors. SRSF1 and hnRNP H (ovals) are fused to the artificial MS2 coat protein (an inverted U shape). MS2 coat protein-binding hairpin RNA is substituted for the splicing regulatory site of exon 16 to directly tether MS2 coat protein-fused SRSF1 and hnRNP H. RT-PCR of pCI-*COLQ*-MS2 minigenes in HeLa cells that are co-transfected with the indicated effectors. A representative gel image of three independent experiments is shown.

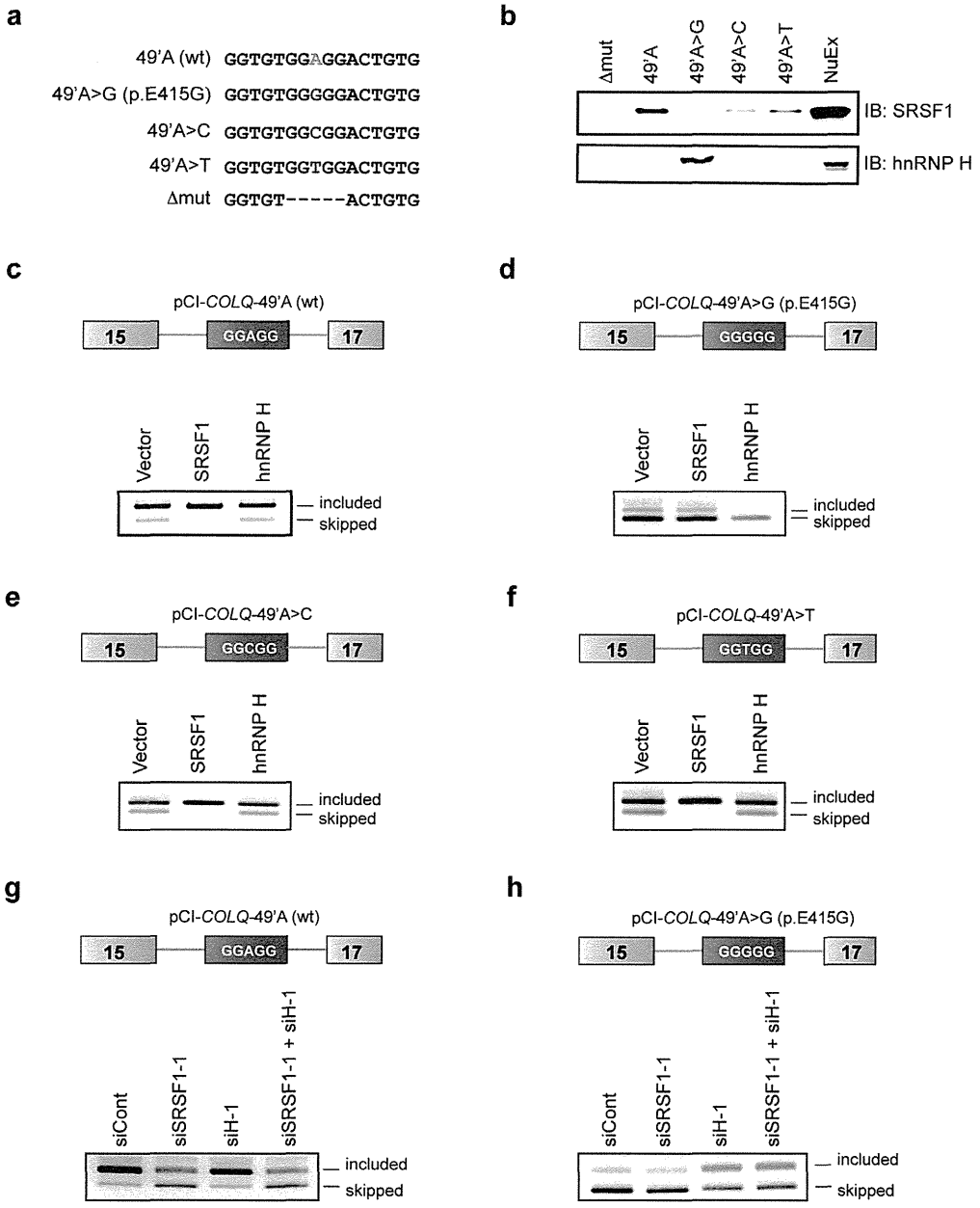

Figure 4. Molecular basis of binding and functional regulation of SRSF1 and hnRNP H. (**a**) Sequences of RNA probes carrying wild-type nucleotide (A), the patient's mutation (G), and artificial mutations (C, T, and Δmut) in *COLQ* exon 16. (**b**) Immunoblots (IB) of RNA affinity-purified proteins bound to each RNA probe. NuEX indicates 5% of the nuclear extract used in the assay. (**c–h**) RT-PCR of pCI-*COLQ* minigenes harboring the indicated motifs that are co-transfected with the indicated *trans*-factors (**c–f**) or siRNAs (**g**,**h**) in HeLa cells. Representative gel images of two independent experiments are shown.

p.E415G impairs splicing of the downstream intron by disrupting SRSF1-induced recruitment of U1 snRNP 70K to the downstream 5′ splice site. We next asked if the p.E415G mutation compromises removal of the upstream or downstream intron. We constructed two sets of minigenes, both of which carried either wild-type (wt) or mutant (p.E415G) sequence. The structure of upstream set was "exon 15-intron 15-exon 16" (E15E16-wt and E15E16-p.E415G), and that of downstream set was "exon 16-intron 16-exon 17" (E16E17-wt and E16E17-p.E415G). We examined the splicing efficiency of these minigenes in HeLa cells. We found that both E15E16-wt and E15E16-p.E415G were spliced to a similar extent, suggesting that p.E415G has no effect on splicing of the upstream intron (Fig. 5a). In contrast,

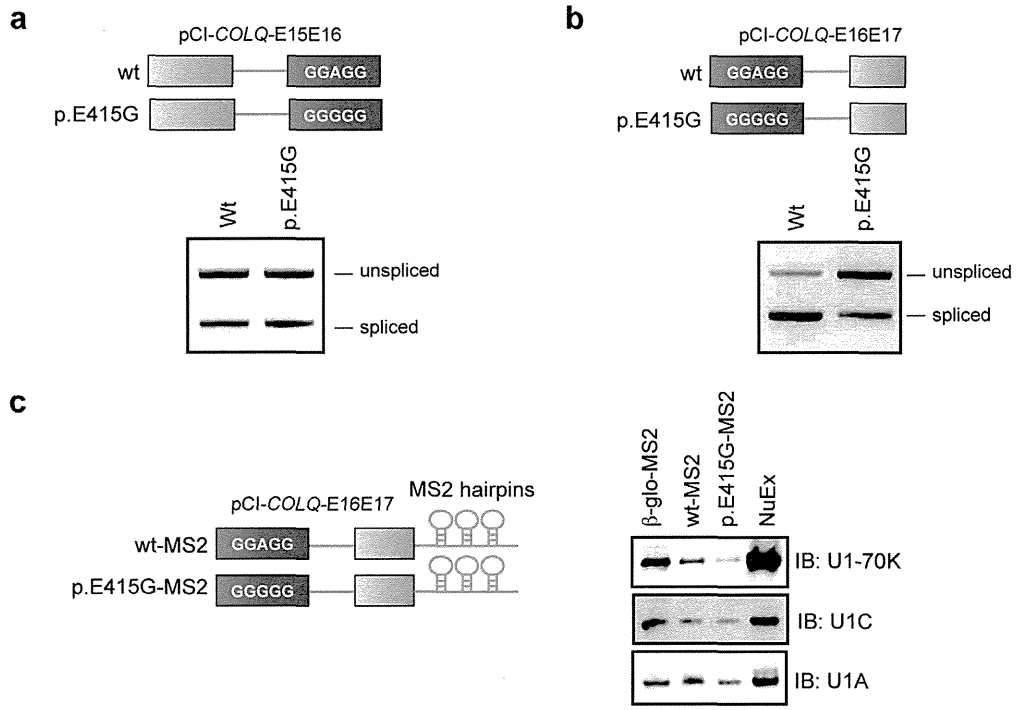

Figure 5. p.E415G compromises recognition of the downstream 5′ splice site by U1-70K. (**a**,**b**) RT-PCR of E15E16 (wt and p.E415G) and E16E17 (wt and p.E415G) minigenes in HeLa cells. (**c**) Schematic structures of MS2-attached wild-type (wt) and p.E415G substrates used for isolation of early spliceosome complex (left). Immunoblotting (IB) of purified spliceosome complex assembled on the indicated substrates (right). β-glo-MS2 is a control construct carrying MS2-attached human β-globin exon 1-intron 1-exon 2[35]. A representative gel image of three independent experiments is shown. Signal intensities of U1-70K bound to wt-MS2 are on average 2.19-fold (SD = 1.21, $n = 3$, $p < 0.05$ by Student's t-test) higher than those bound to p.E415G-MS2.

splicing of E16E17-p.E415G was inefficient compared to E16E17-wt (Fig. 5b), indicating that p.E415G has an inhibitory effect on splicing of the downstream intron.

We next monitored binding of the associated factors (U1 snRNPs) to the downstream 5′ splice site of the wild-type and p.E415G pre-mRNA substrates. We isolated the early spliceosome complex using the MS2-attached wild-type and p.E415G RNA substrates, and analyzed the associated factors by immunoblotting. We found that E16E17-wt-MS2 and β-globin-MS2 efficiently associated with U1 snRNP 70K (U1-70K) (Fig. 5c, lanes 1 and 2). In contrast, association of U1-70K with E16E17-p.E415G-MS2 was less efficient (Fig. 5c, lane 3). There were no appreciable differences in association of U1 snRNP C (U1C) and U1 snRNP A (U1A) between E16E17-wt-MS2 and E16E17-p.E415G-MS2. These observations along with compromised binding of SRSF1 due to p.E415G suggests that SRSF1 likely promotes recruitment of U1 snRNP 70K to the downstream 5′ splice site to achieve efficient inclusion of exon 16.

Global effects of the GGGGG and GGAGG motifs in the human and mouse genomes on pre-mRNA splicing. We next looked into the global significance of the SRSF1-binding GGAGG and hnRNP H-binding GGGGG motifs in the human and mouse genomes. We quantified splicing efficiencies of exons carrying either GGAGG or GGGGG by calculating the percent-spliced-in's (PSI's) of RNA-seq data of the human and mouse brains. In both human and mouse, PSI's of exons carrying GGGGG were significantly lower than those with GGAGG (Fig. 6, Table S3). We also observed a similar tendency in exons flanked by GGGGG- and GGAGG-bearing introns (Fig. S2, Table S3). Thus, a part of human and mouse exons exploit the SRSF1-binding GGAGG and hnRNP H-binding GGGGG motifs to regulate alternative splicing events. It was also interesting to note that human PSI's were lower than mouse PSI's, which supports the notion that humans have evolved by acquiring alternative splicing events.

Discussion

The plasticity and complexity of splicing code enable finely tuned splicing regulation in humans and expand the transcriptome and proteome diversities. However, the increasing splicing complexity predisposes to aberration of splicing regulation that can affect cellular physiology and lead to splicing diseases[29]. Among the numerous splicing codes, ESEs constitute an important class of splicing *cis*-elements

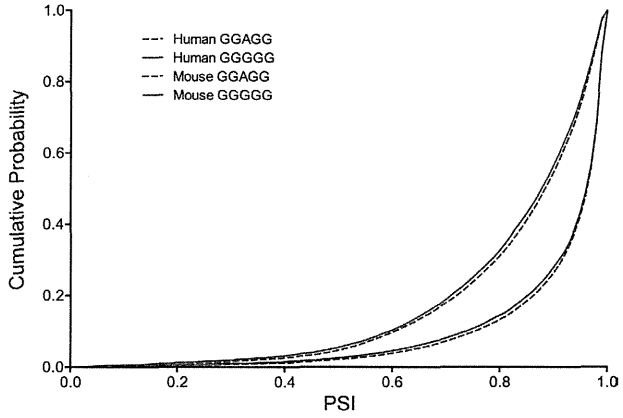

Figure 6. Cumulative distribution function (CDF) plot of PSI's of exons carrying GGGGG or GGAGG that are expressed in the human and mouse brains. PSI is a ratio of inclusion of each exon in the RNA-seq data. CDF is a fraction of exons with PSI's of less than or equal to a specific value. PSI's of exons with GGGGG are shifted to the left compared to those with GGAGG in both human and mouse, indicating that GGGGG-carrying exons are predisposed to be skipped than GGAGG-carrying exons. $P = 0.00003$ between human GGGGG and human GGAGG; $P = 0.00016$ between mouse GGGGG and mouse GGAGG by Student's *t*-test. Mean and SD are indicated in Table S3.

that were acquired in the course of evolution. However, ESEs ironically became vulnerable targets of disease-causing mutations. More than 16–20% of the missense mutations of the human mismatch-repair genes hMSH2 and hMLH1 are predicted to disrupt ESEs and affect splicing of the mutant exons[30]. Therefore, molecular dissection of the effects of ESE-disrupting mutations on RNA splicing is essential to understand disease pathomechanisms and to develop rational therapy to correct splicing errors.

We here investigate the underlying mechanisms of a pathogenic splicing mutation in *COLQ* identified in a patient with endplate AChE deficiency, which causes aberrant skipping of a constitutive exon 16[21]. We demonstrate that the mutation disrupts an ESE and *de novo* generates an ESS to induce exclusive exon skipping. We show that the ESE in *COLQ* exon 16 harbors a high affinity-binding motif for SRSF1. Introduction of artificial mutations in the middle of the core GGAGG motif reveals that SRSF1 preferentially binds to 'A' but not to 'G', 'C', or 'T'. Although binding of SRSF1 to the patient's 'G' mutation is the weakest among the three mutant nucleotides, the difference is marginal. Nevertheless, the 'G' mutation markedly causes exon skipping, whereas the effects of artificial 'C' and 'T' mutations on splicing are moderate. Exclusive binding of hnRNP H to the 'G' mutation is likely to have an additional splicing silencing effect and to account for marked skipping of exon 16. We demonstrate that lack of SRSF1 and gain of hnRNP H is the underlying cause of exclusive skipping of exon 16 in the patient's muscle.

Demonstration of aberrant splicing of *COLQ* not only uncovers the splicing maladies at the patient's endplates, but also allows us to understand SRSF1-mediated splicing regulation under physiological conditions. To further characterize this regulation in cellular context, we examined splicing of endogenous *COLQ* exon 16 in immortalized human myogenic cells (KD3)[31–34] by manipulating the expression levels of SRSF1 and hnRNP H. As expected, overexpression of SRSF1 (Fig. S1c, lane 3) induces inclusion of exon 16 (Fig. S1d, lane 2), whereas overexpression of hnRNP H (Fig. S1c, lane 5) has no effect on splicing of exon 16 (Fig. S1d, lane 3). We also examined the relative expression levels of SRSF1 and hnRNP H in both HeLa and KD3 cells. We found that SRSF1 and hnRNP H are similarly expressed at RNA and protein levels in both KD3 and HeLa cells (Fig. S1e and f). In minigene analysis, we proved that hnRNP H had no effect on splicing of wild-type exon even when SRSF1 is depleted (Fig. 4g). These observations suggest that loss of SRSF1-binding motif (GGAGG) and acquisition of hnRNP H-binding motif (GGGGG) are critical determinants of aberrant skipping *COLQ* exon 16 at the patient's endplates. The patient may somehow overexpress hnRNP H at the endplates, which may have exacerbated aberrant splicing of *COLQ* exon 16.

Point mutation-mediated transition of splicing *trans*-factors and splicing antagonism between two *trans*-factors is also evident in other genes expressed at the NMJ. We reported a point mutation in *CHRNA1* encoding the acetylcholine receptor (AChR) α subunit in a patient with CMS, which switches binding of a splicing-suppressing RNA-binding protein hnRNP L to a splicing-enhancing RNA-binding protein hnRNP LL[35]. The switch induces inclusion of a non-functional exon P3A into *CHRNA1* transcript, which subsequently nullifies expression of AChR on the cell surface and leads to endplate AChR deficiency. In contrast to hnRNPs L and LL in *CHRNA1*, SRSF1 and hnRNP H do not compete for an identical binding site in *COLQ*. Similar antagonistic splicing regulation is also observed in *SMN1* and *SMN2* pre-mRNAs. *SMN1* and *SMN2* are closely related paralogs with only a single nucleotide substitution (C in *SMN1* and T in *SMN2*) at the 6th nucleotide of exon 7. SRSF1 induces inclusion of exon 7

in *SMN1*[36,37]. The C-to-T substitution in *SMN2* gains binding of a splicing-suppressing hnRNP A1[38,39]. Additionally, the C-to-T substitution in *SMN2* may[36,37] or may not[38,39] attenuates binding of SRSF1. Thus, antagonistic splicing regulation by binding of antagonistic splicing *trans*-factors to similar motifs can occur in both physiological and pathological conditions.

Dissection of mechanistic basis of splicing of *COLQ* exon 16 reveals that p.E415G disrupts splicing of the downstream intron, but has no effect on splicing of the upstream intron. Analysis of the purified spliceosome complex reveals that p.E415G inhibits the association of U1 snRNPs in early spliceosome complex by disrupting the recruitment of U1-70K in the downstream 5′ splice site. This suggests that SRSF1 probably enhances recognition of the downstream 5′ splice site of *COLQ* exon 16 by U1 snRNP 70K. Previous studies have repeatedly demonstrated that SRSF1 promotes early spliceosome assembly by interacting with U1-70K[40–43]. The RNA recognition domains (RRM) of SRSF1 promotes the bridging of the RRM of U1-70K to pre-mRNA[40–43], thereby allowing multiple binary interactions including RNA-protein, protein-protein, and RNA-RNA, which are essential for the stability of spliceosomal E complex. Therefore, partial dissociation of U1-70K from spliceosome E complex formed on the p.E415G pre-mRNA substrate is likely due to loss of SRSF1-binding. However, we cannot exclude the possibility that hnRNP H exerts an additional inhibitory effect on recruitment of U1 snRNPs to the 5′ splice site.

Having characterized the antagonistic splicing regulation mediated by SRSF1 and hnRNP H that bind to GGAGG and GGGGG, respectively, we next examined the global antagonistic splicing regulation of the GGAGG and GGGGG motifs in the human and mouse genomes. Analysis of RNA-seq data of the human and mouse brains reveals that exons carrying GGGGG have a higher ratio of exon skipping compared to those carrying GGAGG in both human and mouse. Therefore, the hnRNP H-binding GGGGG motif and the SRSF1-binding GGAGG motif are likely to regulate alternative splicing events in some exons. Thus, a single nucleotide substitution that occurred in the course of evolution potentially increases the proteome diversity by activating or suppressing alternative splicing, and the GGGGG and GGAGG motifs are likely to be a representative pair used in alternative regulation of splicing events.

Materials and Methods

Patient. The current study was in accord with and approved by the Institutional Review Boards of the Mayo Clinic and Nagoya University Graduate School of Medicine. The patient gave written informed consent to participate in the study. The studies were performed in accordance with the relevant guidelines.

Cell culture and transfection. HeLa cells were cultured in the Dulbecco's minimum essential medium (DMEM, Sigma-Aldrich) supplemented with 10% fetal bovine serum (Sigma-Aldrich). HeLa cells were transfected using FuGENE 6 (Roche) according to manufacturer's instructions, unless otherwise indicated. Immortalized human myogenic cells (KD3) were grown and transfected as described previously[31].

Construction of *COLQ* minigene for splicing analysis. To construct a *COLQ* minigene, a 5-kb fragment spanning the 5′ end of exon 15 to the stop codon in exon 17 (Fig. 1c) was amplified by PCR using human genomic DNA isolated from HeLa cells. The forward primer carried an XhoI restriction site followed by the Kozak consensus sequence, 5′-CCACCATG-3′, at the 5′ end. The Kozak sequence was introduced to retain the normal open reading frame of *COLQ*. The reverse primer harbored a NotI restriction site at the 5′ end. The PCR amplicon was cloned into a cytomegalovirus-based expression vector pCI (Promega). The patient's mutation and artificial mutations were engineered into the pCI minigene using the QuikChange Site-Directed Mutagenesis Kit (Stratagene).

RT-PCR for splicing analysis. Total RNA was extracted 40 h after transfection using Trizol (Invitrogen), followed by DNase I treatment. cDNA was synthesized with an oligo-dT primer using ReverTra Ace (Toyobo). PCR amplifications were performed by GoTaq (Promega), using primer pairs 5′-CAGCTGACCCCTTTCTACCC-3′ and 5′-AGCGGCAGGGCGTGGAGT-3′.

RNA affinity purification assay. Biotinylated RNAs were synthesized with the RiboMAX System (Promega) using a PCR-amplified fragment. The PCR-amplicon was generated by annealing two primers followed by overlap extension PCR[44]. Forward primer carried the T7 promoter sequence at the 5′ end. In each 20 μl reaction, 2 μg DNA template was transcribed by T7 RNA polymerase in the presence of 7.5 mM UTP, 7.5 mM ATP, 7.5 mM GTP, 4.5 mM CTP and 3.0 mM Biotin-14-CTP (Invitrogen).

The RNA affinity purification method was slightly modified from the previously reported protocols[35]. Biotinylated RNAs (0.75 nmol) and HeLa nuclear extract (40 μl) (CilBiotech) were mixed in a binding buffer [20 mM HEPES pH 7.8, 150 mM KCl, 0.1 mM EDTA, 1 mM DTT, 1 mM PMSF, 0.05% Triton X, 1 × Protease Inhibitor Cocktail (Active Motif)]. A binding reaction of 500 μl was incubated at 30 °C for 2 h with gentle agitation. In parallel, 50 μl streptavidin-conjugated beads (Streptavidin-sepharose, GE Healthcare) were blocked with a 1:1 mixture of 1 ml binding buffer containing yeast tRNA (0.1 mg/100 μl of beads) and 1 ml PBS containing 4% BSA at 4 °C with rotation for 1 h. After blocking, the beads were washed twice in 1 ml binding buffer and mixed with the binding reaction for 2 h at 4 °C with gentle rotation. After washing the beads four times with 1 ml binding buffer, RNA-bound proteins were harvested

in SDS loading buffer by boiling at 95 °C for 5 min. The purified proteins were fractionated on a 10% SDS-polyacrylamide gel and stained with Coomassie blue or resolved by immunoblotting.

Mass spectrometry. The band of interest was excised from the Coomassie blue-stained gel and processed for in-gel digestion by Trypsin Gold (Promega) according to the manufacturer's protocols. Nanoelectrospray tandem mass analysis was executed using an LCQ Advantage Mass Spectrometry System (Thermo Finnigan) combined with a Paradigm MS4 HPLC System (Michrom BioResources) equipped with a Magic C18AQ column of 0.1 mm in diameter and 50 mm in length (Michrom BioResources). Reversed-phase chromatography was performed with a linear gradient (0 min, 5% B; 45 min, 100% B) of solvent A (2% acetonitrile with 0.1% formic acid) and solvent B (90% acetonitrile with 0.1% formic acid) at an estimated flow rate of 1 μl/min. Ionization was performed with an ADVANCE Captive Spray Source (Michrom BioResources) with a capillary voltage at 1.7 kV and temperature of 150 °C. A precursor ion scan was carried out using a 400–2000 mass to charge ratio (m/z) prior to MS/MS analysis. Multiple MS/MS spectra were resolved by the Mascot program version 2.4.1 (Matrix Science).

siRNA-mediated knocking down and splicing analysis of minigenes. We synthesized siRNA for human SRSF1 with the sequence of 5′-CCAAGGACAUUGAGGACGUTT-3′ (Sigma Genosys). We previously synthesized siRNA for human hnRNP H[26]. To rule out the possible off-target effects, a second set of siRNAs were similarly synthesized: 5′-GGAAAGAAGAUAUGACCUATT-3′ for human SRSF1 and 5′-GGAAGAAAUUGUUCAGUUC-3′ for human hnRNP H. The control siRNA was AllStar Negative Control siRNA (1027281) by Qiagen.

Cells were plated 24 h before transfection in a six-well culture plate (1.5×10^5 cells/well). The transfection reagent included each siRNA duplex at a final concentration of 30 nM in the Opti-MEM medium, 1 μl Lipofectamine 2000 (Invitrogen), and 500 ng of the minigene in 100 μl DMEM. Three days after incubation at 37 °C, the cells were harvested and were subjected to immunoblotting analysis. Total RNA was also isolated from the harvested cells and RT-PCR was performed for splicing analysis.

cDNA overexpression and minigene splicing. To construct an expression vector of human SRSF1, we first amplified human SRSF1 cDNA by RT-PCR using total RNA from human skeletal muscle (Clontech). We then cloned the cDNA amplicon into pCDNA3.1D/V5-His TOPO vector (Invitrogen) according to manufacturer's instructions to obtain pcDNA-SRSF1. The construction of human hnRNP H cDNA in pCDNA3.1D/V5-His TOPO vector (pcDNA-hnRNP H) was previously described[26]. Prior to transfection, cells were plated 24 h in a six-well culture plate (1.5×10^5 cells/well) and transfected with 1 μg of the expression construct, 500 ng of the minigene, and 3.5 μl of FuGENE 6 (Roche) in 100 μl Opti-MEM medium according to the manufacturer's instructions. Three days after incubation at 37 °C, the cells were harvested and were subjected to immunoblotting analysis. For splicing analysis, total RNA was also isolated from the harvested cells and RT-PCR was performed.

Harvesting cells for immunoblotting. Cells were washed twice in PBS and harvested in PBS with 1 × Protease Inhibitor Cocktail. After centrifugation at 2,000 × *g* for 5 min, the pellets were suspended in buffer A (10 mM HEPES-NaOH pH 7.8, 10 mM KCl, 0.1 mM EDTA, 1 mM DTT, 0.5 mM PMSF, 0.1% Nonidet P-40, 1 × Protease Inhibitor Cocktail) and kept for 30 min on ice. Following sonication, samples were centrifuged at 20,000 × *g* for 5 min. The supernatants were collected as total cell lysate.

MS2-mediated artificial tethering of *trans*-factor. Artificial tethering was performed by co-transfection of a reporter minigene and an effector construct as previously described[35]. We introduced the MS2-binding site (5′-ACATGAGGATCACCCATGT-3′)[35] in the minigene by replacing the native target using the QuikChange Site-Directed Mutagenesis Kit, so that effector molecule can bind to the artificially inserted target site in the reporter minigene. To construct pcDNA-SRSF1-MS2, an insert encoding MS2 was isolated from pcDNA-hnRNP L-MS2[35] using XhoI and XbaI restriction enzymes, purified, and cloned into the respective sites of pcDNA-SRSF1. We previously made pcDNA-hnRNP H-MS2 expressing hnRNP H-MS2[26] and pcDNA-MS2 expressing MS2 alone[35].

Splice site function and early spliceosomal complex assays. We constructed E15E16 (wt and p.E415G) minigenes spanning *COL9* exon 15 to 16 and E16E17 (wt and p.E415G) minigenes spanning *COL9* exon 16 to 17 in pcDNA3.1D/V5-His-TOPO vector (Invitrogen). Amplicons were generated by PCR using pCI-*COL9* (wt or p.E415G), and cloned into pcDNA3.1D/V5-His-TOPO vector.

We introduced three copies MS2-coat protein binding hairpin sequences at the 3′ end of E16E17 (wt and E415G) constructs using the megaprimer method[45]. At first, we PCR-amplified a fragment harboring three copies MS2-coat protein binding hairpin sequences from pSP64-MS2 vector[35] with the primers carrying complementary sequences to E16E17 minigene where the MS2-sequences is being inserted. The PCR amplicon was used as a megaprimer for the QuikChange site-directed mutagenesis system. These vectors were used as templates to generate MS2-attached RNA substrates of E16E17 (wt and p.E415G) for isolation of early spliceosomal complex. As control, we used MS2-attached human β-globin exon 1-intron 1-exon 2 construct (pSP64-HβΔ6-MS2) as previously described[35].

MS2-affinity isolation of early spliceosomal complex. One pmol of the RNA probe (β-globin-MS2, E16E17-wt-MS2, or E16E17-p.E415G-MS2) was incubated with a 20-fold molar excess of MS2-MBP fusion protein[46] before mixing it with HeLa nuclear extract. Fifty μl of HeLa nuclear extract was pre-treated with 10 μl (bead volume) of amylose resin (New England Biolabs) overnight at 4 °C. The pre-treated HeLa nuclear extract was incubated at 37 °C for 30 min with a mixture of the RNA probe and the MS2-MBP fusion protein at final concentrations of 60 mM KCl and 25% HeLa nuclear extract. Then amylose resin beads (20 μl) was added in the mixture and incubated at 4 °C for 30 min with gentle rotation. After washing the resin four times with wash a buffer (20 mM HEPES pH 8.0, 150 mM KCl, and 0.05% Triton X-100), bound proteins were eluted with 10 mM maltose solution and subjected to SDS-PAGE followed by immunoblot analyses.

Analysis of the GGGGG and GGAGG motifs in the human and mouse genomes. To understand the effects of the SRSF1-binding GGAGG motif and hnRNP H-binding GGGGG motif on pre-mRNA splicing in the human and mouse genomes, we analyzed RNA-seq of the brains of human (Illumina BodyMap 2.0 at http://www.ebi.ac.uk/arrayexpress/experiments/E-MTAB-513/) and mouse[47]. RNA-seq of human and mouse brains had 63,966,169 and 93,246,802 paired-end reads, respectively. RNA-seq fastq files were mapped to the human genome hg19/GRCh37 or the mouse genome mm9 using TopHat version 2.0.12[48]. The mapping efficiency was 87.0% and 78.5%, respectively. The mapped reads were analyzed at the transcript level with Cufflinks version 2.2.1[49]. Among 217,852 and 206,107 exons annotated in Ensembl release 65, 114,971 (52.8%) and 128,785 (62.5%) exons were expressed in the human and mouse brains, respectively. The numbers of GGGGG- and GGAGG-bearing exons among the expressed exons are shown in Supplementary Table S1. The copy numbers of GGGGG- and GGAGG-motifs within an exon are shown in Supplementary Table S2. The percent-spliced-in (PSI) values of the expressed exons carrying GGGGG or GGAGG were calculated using MISO version 0.5.2[50]. We compared PSI values of the motif-bearing and motif-lacking exons. Cumulative distribution functions were plotted with Prism 6.0f (GraphPad software).

Antibodies. Antibodies used in this study were anti-SRSF1 (32–4500, Invitrogen), anti-U1-snRNP 70K (U1-70K) (H111, kindly provided by Akila Mayeda, Division of Gene Expression Mechanism, Fujita Health University), anti-U1 snRNP C (U1C) (4H12, Sigma-Aldrich), anti-U1 snRNP A (U1A) (PA5-27474, Thermo Fisher Scientific Pierce), anti-His-tag (D293-1, Medical & Biological Laboratories) and anti-GAPDH (Sigma-Aldrich).

References

1. Engel, A. G., Ohno, K. & Sine, S. M. Sleuthing molecular targets for neurological diseases at the neuromuscular junction. *Nat Rev Neurosci* **4,** 339–352 (2003).
2. Engel, A. G. Current status of the congenital myasthenic syndromes. *Neuromuscul Disord* **22,** 99–111 (2012).
3. Hall, Z. W. Multiple forms of acetylcholinesterase and their distribution in endplate and non-endplate regions of rat diaphragm muscle. *J Neurobiol* **4,** 343–361 (1973).
4. Ohno, K., Brengman, J., Tsujino, A. & Engel, A. G. Human endplate acetylcholinesterase deficiency caused by mutations in the collagen-like tail subunit (ColQ) of the asymmetric enzyme. *Proc Natl Acad Sci USA* **95,** 9654–9659 (1998).
5. Ohno, K., Ohkawara, B., Ito, M. & Engel, A. G. Molecular Genetics of Congenital Myasthenic Syndromes. in *eLS* doi: 10.1002/9780470015902.a9780470024314 (John Wiley & Sons, Inc., 2014).
6. Ohno, K. *et al.* The spectrum of mutations causing endplate acetylcholinesterase deficiency. *Ann Neurol* **47,** 162–170 (2000).
7. Peng, H. B., Xie, H., Rossi, S. G. & Rotundo, R. L. Acetylcholinesterase clustering at the neuromuscular junction involves perlecan and dystroglycan. *J Cell Biol* **145,** 911–921 (1999).
8. Cartaud, A. *et al.* MuSK is required for anchoring acetylcholinesterase at the neuromuscular junction. *J Cell Biol* **165,** 505–515 (2004).
9. Ito, M. *et al.* Protein-anchoring strategy for delivering acetylcholinesterase to the neuromuscular junction. *Mol Ther* **20,** 1384–1392 (2012).
10. Engel, A. G. The therapy of congenital myasthenic syndromes. *Neurotherapeutics* **4,** 252–257 (2007).
11. Liewluck, T., Selcen, D. & Engel, A. G. Beneficial Effects of Albuterol in Congenital Endplate Acetylcholinesterase Deficiency and Dok-7 Myasthenia. *Muscle Nerve* **44,** 789–794 (2011).
12. Pandit, S. *et al.* Genome-wide analysis reveals SR protein cooperation and competition in regulated splicing. *Mol Cell* **50,** 223–235 (2013).
13. Zhang, Z. & Krainer, A. R. Involvement of SR proteins in mRNA surveillance. *Mol Cell* **16,** 597–607 (2004).
14. Huang, C. *et al.* Characterization and *in vivo* functional analysis of splice variants of cypher. *J Biol Chem* **278,** 7360–7365 (2003).
15. Sun, S., Zhang, Z., Sinha, R., Karni, R. & Krainer, A. R. SF2/ASF autoregulation involves multiple layers of post-transcriptional and translational control. *Nat Struct Mol Biol* **17,** 306–312 (2010).
16. Karni, R. *et al.* The gene encoding the splicing factor SF2/ASF is a proto-oncogene. *Nat Struct Mol Biol* **14,** 185–193 (2007).
17. Han, K., Yeo, G., An, P., Burge, C. B. & Grabowski, P. J. A combinatorial code for splicing silencing: UAGG and GGGG motifs. *PLoS Biol* **3,** 843–860 (2005).
18. Chou, M. Y., Rooke, N., Turck, C. W. & Black, D. L. hnRNP H is a component of a splicing enhancer complex that activates a c-src alternative exon in neuronal cells. *Mol Cell Biol* **19,** 69–77 (1999).
19. Caputi, M. & Zahler, A. M. SR proteins and hnRNP H regulate the splicing of the HIV-1 tev-specific exon 6D. *EMBO J* **21,** 845–855 (2002).
20. Wang, E. M., Dimova, N. & Cambi, F. PLP/DM20 ratio is regulated by hnRNPH and F and a novel G-rich enhancer in oligodendrocytes. *Nucleic Acids Res* **35,** 4164–4178 (2007).
21. Kimbell, L. M., Ohno, K., Engel, A. G. & Rotundo, R. L. C-terminal and heparin-binding domains of collagenic tail subunit are both essential for anchoring acetylcholinesterase at the synapse. *J Biol Chem* **279,** 10997–11005 (2004).
22. Nakata, K. *et al.* DISC1 splice variants are upregulated in schizophrenia and associated with risk polymorphisms. *Proc Natl Acad Sci USA* **106,** 15873–15878 (2009).

23. Liu, X. D. & Mertz, J. E. Hnrnp-L Binds a Cis-Acting Rna Sequence Element That Enables Intron-Independent Gene-Expression. *Genes Dev* **9,** 1766–1780 (1995).
24. Sanford, J. R. *et al.* Splicing factor SFRS1 recognizes a functionally diverse landscape of RNA transcripts. *Genome Res* **19,** 381–394 (2009).
25. Caputi, M. & Zahler, A. M. SR proteins and hnRNP H regulate the splicing of the HIV-1 tev-specific exon 6D. *EMBO J* **21,** 845–855 (2002).
26. Masuda, A. *et al.* hnRNP H enhances skipping of a nonfunctional exon P3A in CHRNA1 and a mutation disrupting its binding causes congenital myasthenic syndrome. *Hum Mol Genet* **17,** 4022–4035 (2008).
27. Huelga, S. C. *et al.* Integrative genome-wide analysis reveals cooperative regulation of alternative splicing by hnRNP proteins. *Cell Rep* **1,** 167–178 (2012).
28. Liu, H. X., Zhang, M. & Krainer, A. R. Identification of functional exonic splicing enhancer motifs recognized by individual SR proteins. *Genes Dev* **12,** 1998–2012 (1998).
29. Cooper, T. A., Wan, L. & Dreyfuss, G. RNA and disease. *Cell* **136,** 777–793 (2009).
30. Gorlov, I. P., Gorlova, O. Y., Frazier, M. L. & Amos, C. I. Missense mutations in hMLH1 and hMSH2 are associated with exonic splicing enhancers. *Am J Hum Genet* **73,** 1157–1161 (2003).
31. Nasrin, F. *et al.* HnRNP C, YB-1 and hnRNP L coordinately enhance skipping of human MUSK exon 10 to generate a Wnt-insensitive MuSK isoform. *Sci Rep* **4,** 6841 (2014).
32. Shiomi, K. *et al.* CDK4 and cyclin D1 allow human myogenic cells to recapture growth property without compromising differentiation potential. *Gene Ther* **18,** 857–866 (2011).
33. Wada, M. R., Inagawa-Ogashiwa, M., Shimizu, S., Yasumoto, S. & Hashimoto, N. Generation of different fates from multipotent muscle stem cells. *Development* **129,** 2987–2995 (2002).
34. Hashimoto, N. *et al.* Immortalization of human myogenic progenitor cell clone retaining multipotentiality. *Biochem Biophys Res Commun* **348,** 1383–1388 (2006).
35. Rahman, M. A. *et al.* HnRNP L and hnRNP LL antagonistically modulate PTB-mediated splicing suppression of CHRNA1 pre-mRNA. *Sci Rep* **3,** 2931 (2013).
36. Cartegni, L., Hastings, M. L., Calarco, J. A., de Stanchina, E. & Krainer, A. R. Determinants of exon 7 splicing in the spinal muscular atrophy genes, SMN1 and SMN2. *Am J Hum Genet* **78,** 63–77 (2006).
37. Cartegni, L. & Krainer, A. R. Disruption of an SF2/ASF-dependent exonic splicing enhancer in SMN2 causes spinal muscular atrophy in the absence of SMN1. *Nat Genet* **30,** 377–384 (2002).
38. Kashima, T. & Manley, J. L. A negative element in SMN2 exon 7 inhibits splicing in spinal muscular atrophy. *Nat Genet* **34,** 460–463 (2003).
39. Kashima, T., Rao, N., David, C. J. & Manley, J. L. hnRNP A1 functions with specificity in repression of SMN2 exon 7 splicing. *Hum Mol Genet* **16,** 3149–3159 (2007).
40. Kohtz, J. D. *et al.* Protein-protein interactions and 5′-splice-site recognition in mammalian mRNA precursors. *Nature* **368,** 119–124 (1994).
41. Xiao, S. H. & Manley, J. L. Phosphorylation of the ASF/SF2 RS domain affects both protein-protein and protein-RNA interactions and is necessary for splicing. *Genes Dev* **11,** 334–344 (1997).
42. Cao, W. H. & Garcia-Blanco, M. A. A serine/arginine-rich domain in the human U1 70k protein is necessary and sufficient for ASF/SF2 binding. *J Biol Chem* **273,** 20629–20635 (1998).
43. Cho, S. Y. *et al.* Interaction between the RNA binding domains of Ser-Arg splicing factor 1 and U1-70K snRNP protein determines early spliceosome assembly. *Proc Natl Acad Sci USA* **108,** 8233–8238 (2011).
44. Higuchi, R., Krummel, B. & Saiki, R. K. A general method of *in vitro* preparation and specific mutagenesis of DNA fragments: study of protein and DNA interactions. *Nucleic Acids Res* **16,** 7351–7367 (1988).
45. Ohno, K. *et al.* Myasthenic syndromes in Turkish kinships due to mutations in the acetylcholine receptor. *Ann Neurol* **44,** 234–241 (1998).
46. Das, R., Zhou, Z. & Reed, R. Functional association of U2 snRNP with the ATP-independent spliceosomal complex E. *Mol Cell* **5,** 779–787 (2000).
47. Merkin, J., Russell, C., Chen, P. & Burge, C. B. Evolutionary dynamics of gene and isoform regulation in Mammalian tissues. *Science* **338,** 1593–1599 (2012).
48. Trapnell, C., Pachter, L. & Salzberg, S. L. TopHat: discovering splice junctions with RNA-Seq. *Bioinformatics* **25,** 1105–1111 (2009).
49. Trapnell, C. *et al.* Transcript assembly and quantification by RNA-Seq reveals unannotated transcripts and isoform switching during cell differentiation. *Nat Biotechnol* **28,** 511–515 (2010).
50. Katz, Y., Wang, E. T., Airoldi, E. M. & Burge, C. B. Analysis and design of RNA sequencing experiments for identifying isoform regulation. *Nat Methods* **7,** 1009–1015 (2010).
51. Zhang, M. Q. Statistical features of human exons and their flanking regions. *Hum Mol Genet* **7,** 919–932 (1998).

Acknowledgments

We thank Kentaro Taki (Nagoya University Graduate School of Medicine) for his technical assistance on the mass spectrometry analysis. We are grateful to Robin Reed (Harvard Medical School, Boston, MA) for kindly providing MS2-MBP fusion protein construct; Akila Mayeda (Fujita Health University, Toyoake, Japan) for U1-70K (H111) antibody; and Naohiro Hashimoto (National Center for Geriatrics and Gerontology, Obu, Japan) for KD3 cells. This work was supported by Grants-in-Aid from the MEXT and MHLW of Japan to AM and KO and by NIH Grant NS6277 to AGE.

Author Contributions

K.O. and A.G.E. conceived the project. M.A.R. and A.M. designed experiments; M.A.R. performed most of the experiments with the help of Y.A., F.N., M.N., K.B.A. and J.T. performed *in silico* analyses; M.A.R., A.G.E. and K.O. wrote the paper.

Additional Information

Supplementary information accompanies this paper at http://www.nature.com/srep

Competing financial interests: The authors declare no competing financial interests.

How to cite this article: Rahman, M. A. *et al.* SRSF1 and hnRNP H antagonistically regulate splicing of *COLQ* exon 16 in a congenital myasthenic syndrome. *Sci. Rep.* **5**, 13208; doi: 10.1038/srep13208 (2015).

INTERNAL MEDICINE

□ PICTURES IN CLINICAL MEDICINE □

Sporadic Inclusion Body Myositis Presenting with Beevor's Sign

Kazuma Sugie, Aya Kumazawa and Satoshi Ueno

Key words: Beevor's sign, protuberant abdomen, sporadic inclusion body myositis (sIBM)

(Intern Med 54: 2793-2794, 2015)
(DOI: 10.2169/internalmedicine.54.5002)

Picture 1.

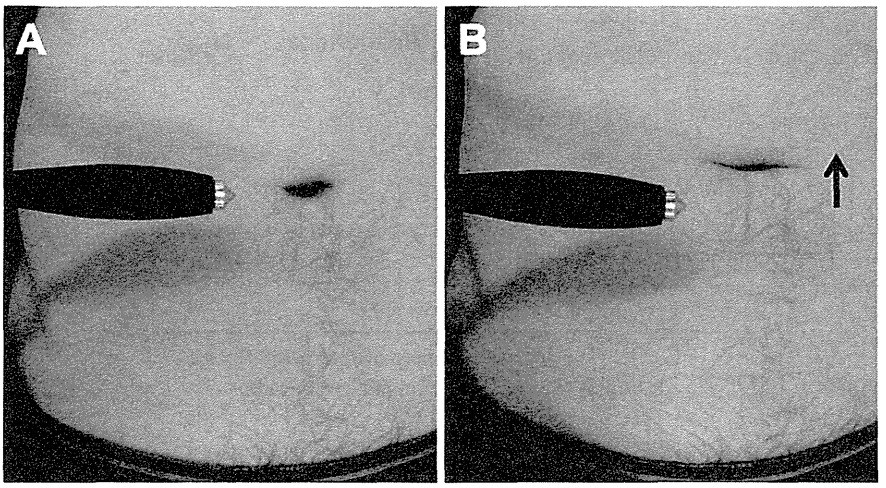

Picture 2.

Department of Neurology, Nara Medical University School of Medicine, Japan
Received for publication January 21, 2015; Accepted for publication March 5, 2015
Correspondence to Dr. Kazuma Sugie, ksugie@naramed-u.ac.jp

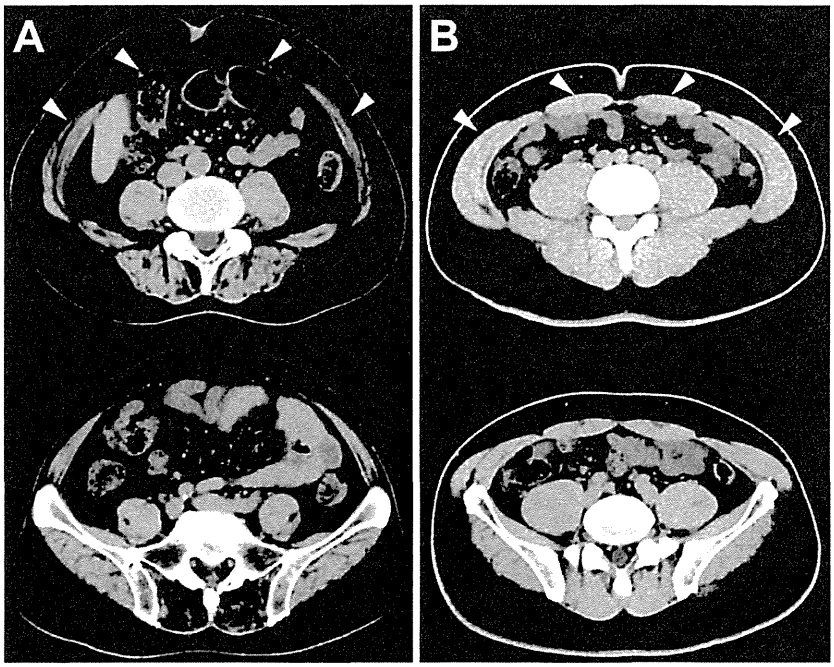

Picture 3.

A 61-year-old man with a four-year-history of sporadic inclusion body myositis (sIBM) presented with progressive quadriceps and finger flexor muscle weakness. He was given a definitive diagnosis of sIBM based on a muscle biopsy. Recently, he developed weak abdominal muscles with a protuberant abdomen (Picture 1) and positive Beevor's sign without spinal lesions [Picture 2, before (A) and after (B) neck flexion]. CT showed marked atrophy and fatty replacement of the rectus abdominis muscle and abdominal oblique muscles (arrowheads in Picture 3A), as compared with that observed in an age-matched healthy male control (Picture 3B).

sIBM is a type of inflammatory myopathy characterized by both degenerative and autoimmune features. Beevor's sign, upward movement of the umbilicus with a supine flexing neck due to paralysis of the inferior portion of the abdominal muscles and a protuberant abdomen are usually observed in patients with facioscapulohumeral dystrophy (1, 2), although these features have not been previously reported in cases of sIBM. This observation suggests that the presence of Beevor's sign emphasizes the need to consider sIBM with protuberant abdomen in the differential diagnosis and that sIBM is more clinically variable than previously thought.

The authors state that they have no Conflict of Interest (COI).

References

1. Venance SL, Tawil R. Facioscapulohumeral muscular dystrophy. In: Disorders of Voluntary Muscle. 8th ed. Karpati G, Hilton-Jones D, Bushby K, Griggs RC, Eds. Cambridge University Press, Cambridge, 2010: 314-322.
2. Eger K, Jordan B, Habermann S, Zierz S. Beevor's sign in facioscapulohumeral muscular dystrophy: an old sign with new implications. J Neurol **257**: 436-438, 2010.